Source Modelling and Strong Ground Motion of the 2011 Tohoku Earthquake

Hidenori Kawabe, Katsuhiro Kamae, Hirotoshi Uebayashi
Research Reactor Institute, Kyoto University, Japan

15 WCEE
LISBOA 2012

SUMMARY:
The 2011 Tohoku earthquake of 11 March 2011 occurred in the subduction zone plate boundary between the Pacific and North American plates along the Japan Trench. In this study, we try to estimate the source model and simulate the strong ground motions of this earthquake. First of all, we try to estimate the source model by a forward-modeling approach based on the characterized source model using the empirical Green's function method. Based on the results, we proposed a source model composed of five strong motion generation areas on the subducting plate boundary. Next, we performed a strong ground motion simulation using the 3D finite-difference method. Our simulation target area was the region from Miyagi Prefecture to the Kanto basin. The effective period of this simulation is from 3 to 10 sec. The resulting S wave amplitude and arrival time of synthetic waveforms are in good agreement with the observed ones.

Keywords: Strong ground motion, Source modeling, Subduction zoon earthquake, Finite difference method

1. INTRODUCTION

On 11 March 2011, Japan was struck by a massive Mw 9.0 subduction zone earthquake whose epicenter was off Miyagi Prefecture in the Tohoku region (the 2011 Tohoku earthquake). The source area extends approximately 400 km along the Japan trench. The seismic ground motions of this earthquake caused severe damage and casualties over a wide area from Tohoku into the Kanto region. Eastern Japan was also struck by a tsunami, wreaking catastrophic damage to coastal areas.

Many strong motion records of this earthquake were obtained by the strong motion observation networks in Japan. The duration of observed strong ground motions was quite long. The long-period strong ground motions associated with this earthquake had less effect on high rise buildings than one would expect from the scale of the event. Nevertheless, skyscrapers suffered some ceiling collapses and damage to internal furnishings, elevators and other equipment. It is important to estimate the amplification characteristics, attenuation characteristics and other propagation parameters of the long-period strong ground motions associated with this earthquake to investigate measures that can be taken against such ground motions in future huge earthquakes.

The first of our objectives is to estimate the source model of the 2011 Tohoku earthquake using a forward-modeling procedure. Another of our objectives is to investigate how well the observed long-period strong ground motions during the earthquake are reproduced using our source model and the 3D subsurface structure model proposed by the Headquarters for Earthquake Research Promotion (HERP).

2. STRONG MOTION RECORDS

The 2011 Tohoku earthquake was recorded by well over 1000 strong motion instruments of the National Research Institute for Earth Science and Disaster Prevention (NIED) and other organizations. Fig. 1 shows the ground acceleration records observed by KiK-net strong motion seismograph networks belonging to NIED. These acceleration waveforms indicate two characteristic wave packets in the region north of Miyagi Prefecture. In addition to these two wave packets, different characteristic wave packets are observed in the waveforms observed in Fukushima Prefecture. In Ibaraki Prefecture, a single characteristic wave packet is observed. These waveforms suggest that the source process of this earthquake was extremely complicated.

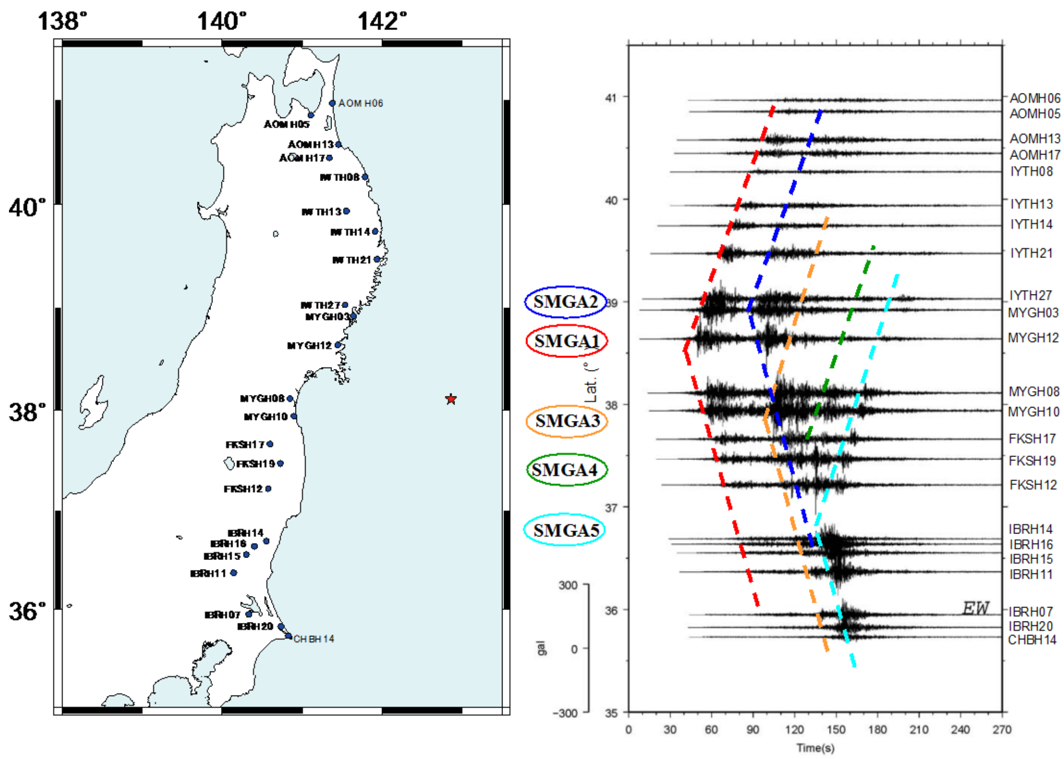

(a) Locations of epicenter and observation stations (b) Acceleration waveforms

Figure 1. Map of the Epicenter (a Red Star) of the 2011 Tohoku Earthquake, KiK-net Strong-Motion Stations and Observed Waveforms at the Bottom of Boreholes (Band Pass Filter: 0.1–10 Hz). Dashed lines represent propagation of 5 wave packets.

3. SOURCE MODELING

In this section, we estimate the source model by a forward-modeling approach, based on the characterized source model using the empirical Green's function method (Irikura, 1986). Using the bandpass-filtered (0.1–10 Hz) subsurface records of KiK-net near the coast, strong motion generation areas (SMGAs) were designated. Considering the shape of the subducting Pacific Plate, the fault plane for this earthquake was assumed to pass through the hypocenter determined by the Japan Meteorological Agency (JMA) with a strike of 195° and dip of 13°. The records from the 4 events listed in Table 1 were used as the empirical Green's functions. The records at the high S-wave velocity layer (see Fig. 2) were used to minimize the influence of amplification of ground motions in the surface layers on the observation records while estimating the source model. Here, the SMGA locations, rupture start times and other parameters were estimated on the basis of the arrival times of the wave packets to each station, based on the wave propagation shown by the dashed line in Fig. 1.

Fig. 2, Fig. 3 and Table 2 show the SMGA locations and source parameters. This source model is composed of five SMGAs located on the sea off Miyagi, south Iwate, Fukushima and Ibaraki Prefectures. Fig. 4 shows examples of comparison between synthetic waveforms calculated by the empirical Green's function method with the observed waveforms. From this figure, it can be seen that the observed waveforms are well reproduced at each observation station.

Table 1. Source Parameters for Small Events

	Event 1	Event 2	Event 3	Event 4
Origin Time (JST)*	2005/12/17 3:32	2011/3/10 3:16	2010/6/13 12:32	2005/10/19 20:44
Latitude (deg.)*	38.449	38.271	37.396	36.382
Longitude (deg.)*	142.181	142.879	141.796	141.043
Depth (km)*	39.9	28.9	40.3	48.3
Mj*	6.1	6.4	6.2	6.3
Mo (Nm)**	1.12×10^{18}	1.10×10^{18}	7.94×10^{17}	3.18×10^{18}
Strike/dip/rake** (deg.)	20/72/91 196/19/86	22/71/90 201/19/89	247/47/72 92/46/108	25/68/88 209/22/94

*JMA, **F-net

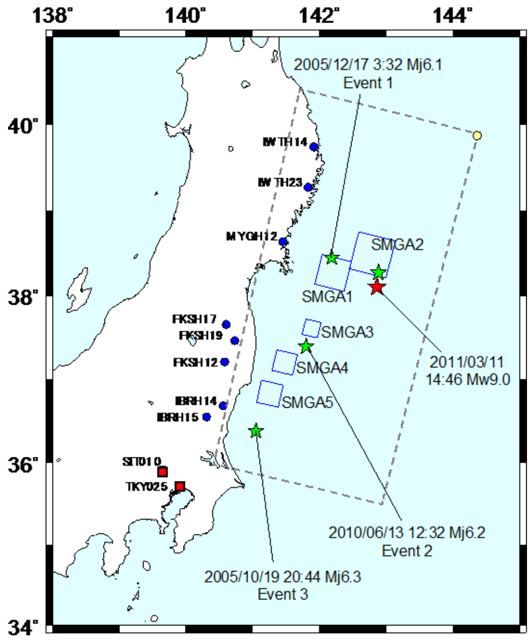

Figure 2. Locations of Epicenters, Strong Motion Generation Areas and Seismic Stations.

Table 2. Source Parameters for SMGAs

		SMGA1	SMGA2	SMGA3	SMGA4	SMGA5
Strike	(°)	195	195	195	195	195
Dip	(°)	13	13	13	13	13
Area	(km^2)	40×40	50×50	21×21	28×28	30×30
Mo	(N•m)	5.02×10^{20}	1.10×10^{21}	6.43×10^{19}	1.02×10^{20}	2.58×10^{20}
Stress Drop	(MPa)	20.4	21.6	15.7	10.5	23.1
Rise Time	(s)	3.6	4.5	1.9	2.5	2.7
Ruptur start time	(s)	0.0	35.0	57.0	87.0	102.0
Empirical Green's function		2005/12/17 3:32 M6.1	2011/03/10 3:16 M6.4	2010/06/13 12:33 M6.2	2010/06/13 12:33 M6.2	2005/10/19 20:44 M6.3

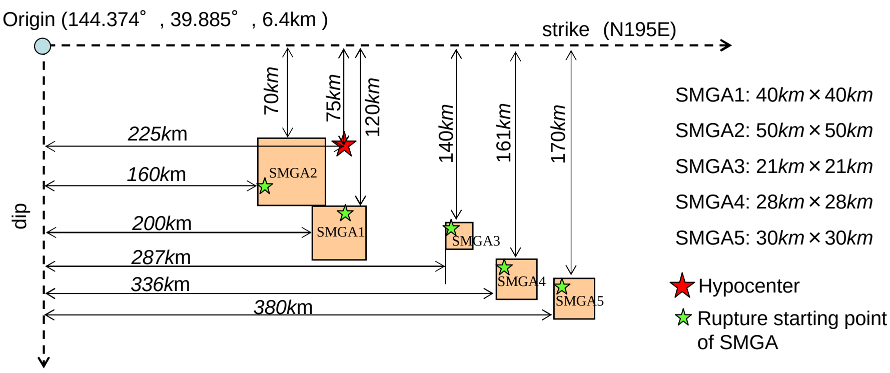

Figure 3. Source Model

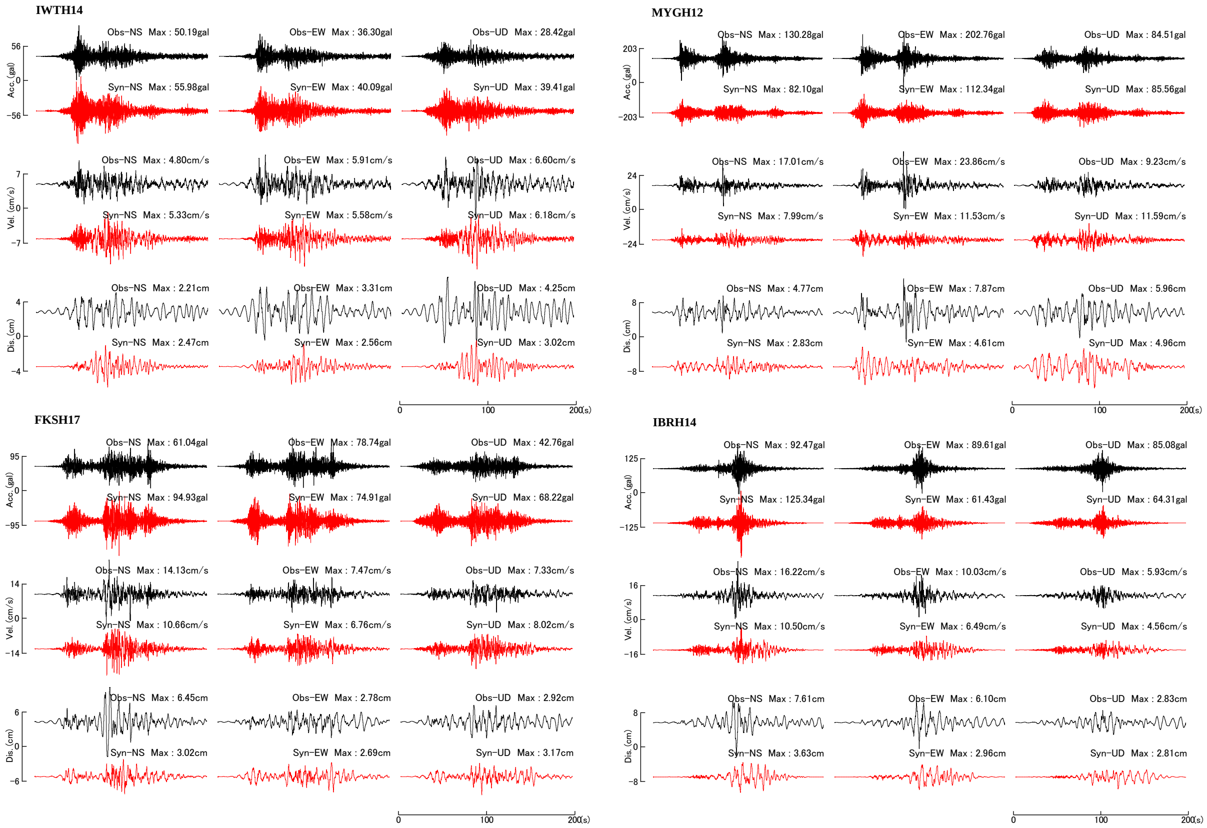

Figure 4. Comparison of Observed (Black Lines) and Calculated (Red Lines) Waveforms for Observation Stations Using Forward Source Modeling (Band Pass Filter: 0.1–10 Hz)

Fig. 5 shows a comparison between observed waveforms by K-NET of NIED, another observation stations that were not used for source modeling, and the synthetic waveforms calculated by the empirical Green's function method. Although the synthetic displacement amplitudes at observation stations in the Kanto basin are smaller than the observed ones, the synthetic velocity and acceleration waveforms generally reproduce the observed ones.

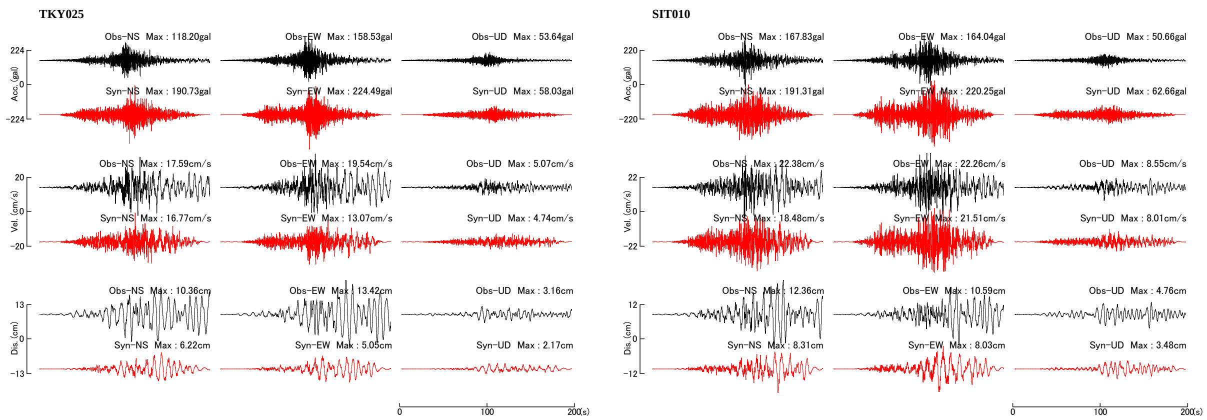

Figure 5. Comparison of Observed (Black Lines) and Calculated (Red Lines) Waveforms for Observation Stations That Was not Used for Source Modeling (Band Pass Filter: 0.1–10 Hz)

4. GROUND MOTION SIMULATION

4.1. Simulation method

Ground-motion simulations were performed using the 3D finite-difference procedure presented by Pitarka (1999). This approach employs a staggered-grid formulation and is applicable to arbitrarily complex 3D elastic media. The algorithm is accurate to fourth order in space and second order in time and allows for the implementation of a finite source with a complex rupture history. We set an absorbing region outside the finite computational region and applied the non-reflecting boundary condition of Cerjan et al. (1985) and the A1 absorbing boundary condition of Clayton and Engquist (1977) to the absorbing region. Anelastic attenuation is accounted for in the simulations by using the technique described by Graves (1996). This approach uses a spatially variable Q operator having a linear dependence on frequency. The surface exposure of the region modeled in the 3D finite-difference simulations is shown in Fig. 6. The finite-difference model covers an area of 412 km (east–west direction) × 471 km (north–south direction), and extends to a depth of 100 km. The grid spacings were 0.3 km horizontally and 0.1 to 0.6 km vertically, and the time step was 0.0075 sec. The absorption region was 20 grids.

The 2012 version subsurface structure model was used in the Long-Period Ground Motion Hazard Map published by HERP (HEAP, 2012). We used the subsurface structure model presented on the HERP website (HERP model). Table 3 shows the physical parameters of the HERP model, and Fig. 7 shows the depth to the top of the basement. The physical parameters for Layer 1 in Table 3 were replaced with the parameters for Layer 2 to carry out the finite-difference calculation.

We used the source model described in Section 3, but the depth of the source model was modified so that the source location would be at the plate boundary in the HERP model. The values for strike and dip angle in Table 2 were used, and the rake angle was assumed to be 90°. The slip velocity time function was calculated using the approximation proposed by Nakamura and Miyatake (2000).

The effective period of the simulation was greater than 3 sec because of the values of the finite-difference grid spacing and the physical parameters of the subsurface structure model. Since the effective period of our source model was 0.1 to 10 sec, the effective period of the synthetic waveforms was 3 to 10 sec.

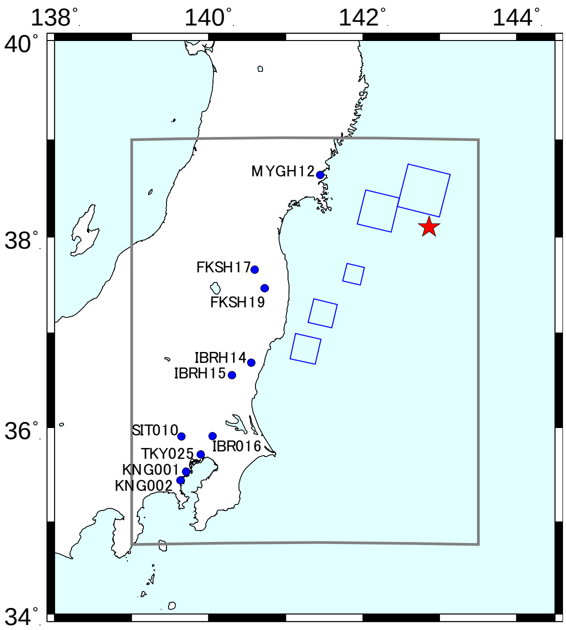

Figure 6. Locations of Finite-Difference Simulation Area, SMGAs and Observation Stations

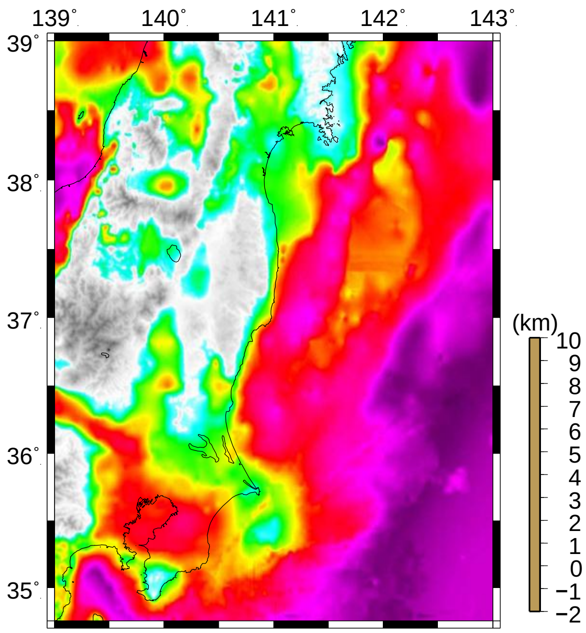

Figure 7. Depth to the Top of Basement for HERP Model.

4.2. Simulation Results

Fig. 8 compares the observed waveforms with the synthetic waveforms. Overall, the propagations of seismic ground motion (such as the arrival time and duration) from the north into the Kanto basin were reproduced. A more detailed look at these results indicates that the amplitude of the principal motions and shape of the wave packet are reproduced from station MYGH12 in Miyagi Prefecture to IBR016 in Ibaraki Prefecture, but the amplitude of the later phase of the synthetic waveforms is somewhat lower than that of the observed ones. The principal motions of the synthetic waveforms correspond

Table 3. Physical Parameters for Subsurface Structure Model (HERP Model)

Layer Num.	Vp (km/s)	Vs (km/s)	ρ (g/cm^3)	Qs	Remarks
1	1.7	0.35	1.80	70	
2	1.8	0.5	1.95	100	
3	2.0	0.6	2.00	120	
4	2.1	0.7	2.05	140	
5	2.2	0.8	2.07	160	
6	2.3	0.9	2.10	180	
7	2.4	1.0	2.15	200	Accretionary Wedge
8	2.7	1.3	2.20	260	
9	3.0	1.5	2.25	300	
10	3.2	1.7	2.30	340	
11	3.5	2.0	2.35	400	
12	4.2	2.4	2.45	400	
13	5.0	2.9	2.60	400	
14	5.5	3.2	2.65	400	Basement (Upper Crust 1)
15	5.8	3.4	2.70	400	Upper Crust 2
16	6.4	3.8	2.80	400	Lower Crust
17	7.5	4.5	3.20	500	Mantle
18	5.0	2.9	2.40	200	Oceanic Crust 2 (Philippine Sea Plate)
19	6.8	4.0	2.90	300	Oceanic Crust 3 (Philippine Sea Plate)
20	8.0	4.7	3.20	500	Oceanic Mantle (Philippine Sea Plate)
21	5.4	2.8	2.60	200	Oceanic Crust 2 (Pacific Plate)
22	6.5	3.5	2.80	300	Oceanic Crust 3 (Pacific Plate)
23	8.1	4.6	3.40	500	Oceanic Mantle (Pacific Plate)

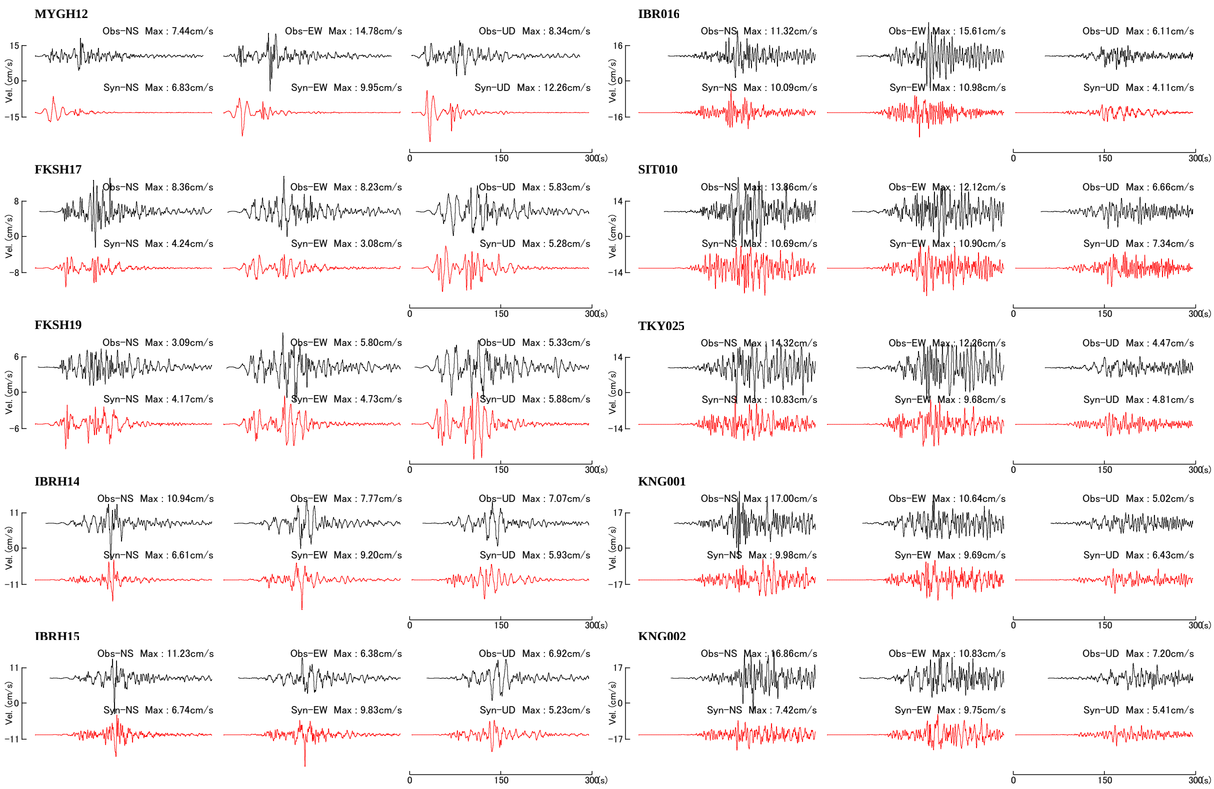

Figure 8. Comparison of Observed (Black Lines) and Calculated (Red Lines) Waveforms for Finite-Difference Simulation (Band Pass Filter: 0.1–0.33 Hz).

well to the observed values for all of the observation stations in the Kanto basin south of the SIT010 station in Saitama Prefecture. In addition, not only the amplitudes but also the phases of the UD components of the observed waveforms are well reproduced by the synthetic waveforms. However, the later phase amplitudes of the synthetic waveform are lower than the amplitudes observed at the stations in Kanto basin. One possible reason for this is that the source model was composed of only five SMGAs, the radiation of ground motions from the other source region was not assumed. It is also possible that the attenuation parameters in the sedimentary basins might be incorrect. These factors will be investigated in a future study. Fig. 9 shows the maximum ground velocities observed by K-NET and KiK-net (surface) stations, and Fig. 10 shows the estimated maximum velocities. It can be seen that there are large horizontal velocities from the Sendai basin to the coastal region of south Fukushima Prefecture and the Kanto basin, whereas the vertical velocities are relatively small in the Kanto basin. These trends are reproduced in the synthetic waveforms shown in Fig. 10. But the amplitudes of the synthetic waveforms are somewhat underestimated. One possible reason for this underestimate is that only subsurface structures with S-wave velocities above 500 m/s were considered in the finite-difference calculation, while the amplification at the surface structures were neglected. Fig. 11 and 12 respectively show the observed and synthetic pseudo-velocity response spectra for periods of 4, 7 and 10 sec. The spectra in Fig. 11 indicate large amplitudes for periods of 7 and 10 sec

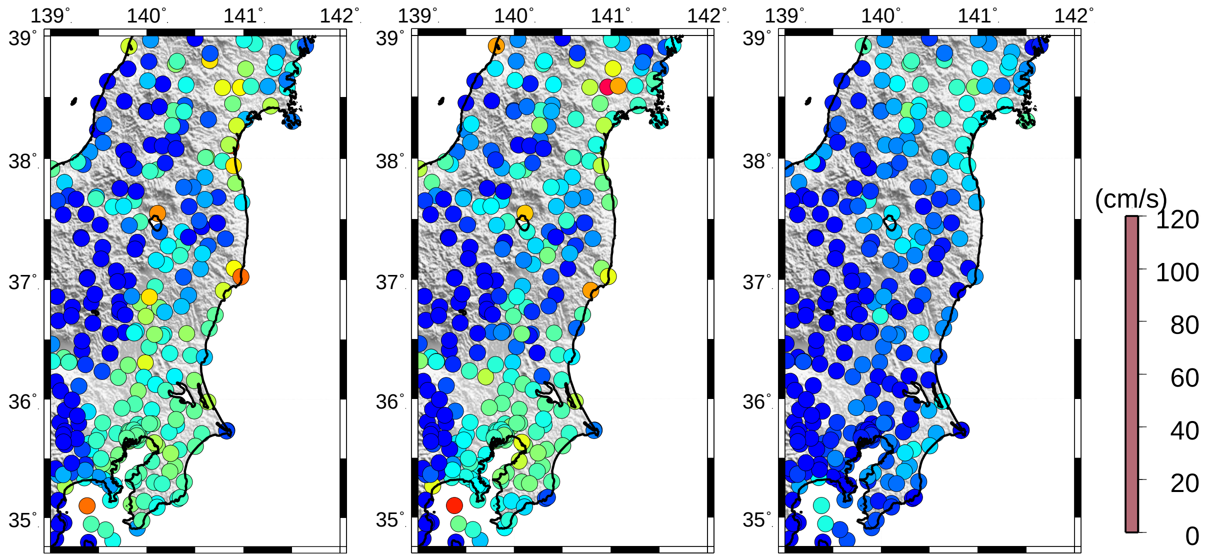

Figure 9. Peak Ground Velocity Observed at the K-NET and KiK-net Stations (Band Pass Filter: 0.1–0.33 Hz)

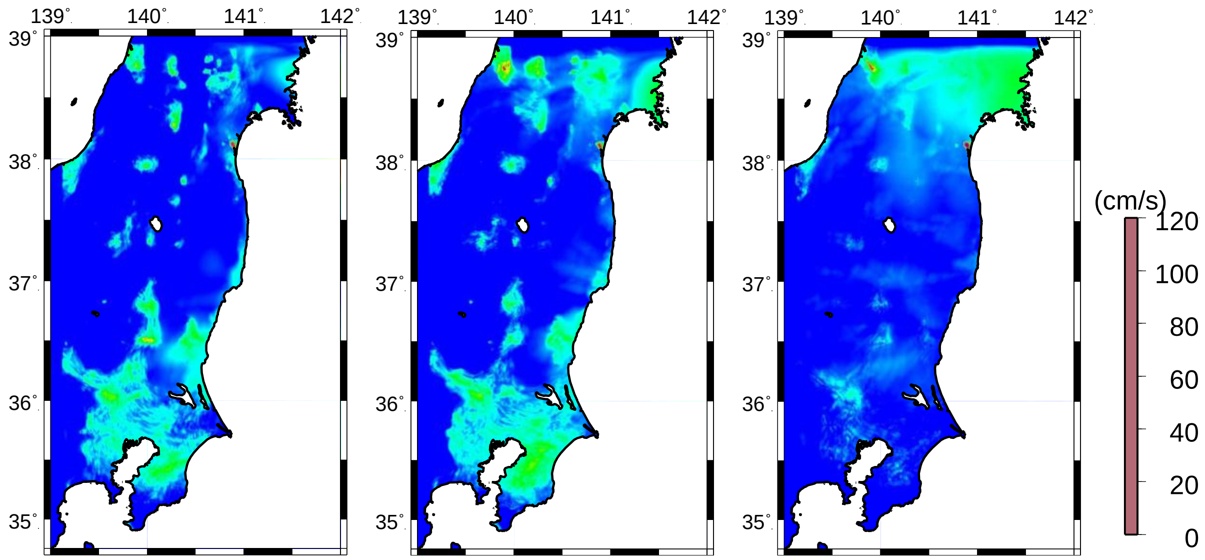

Figure 10. Peak Ground Velocity for Strong Ground Motion Simulation (Band Pass Filter: 0.1–0.33 Hz)

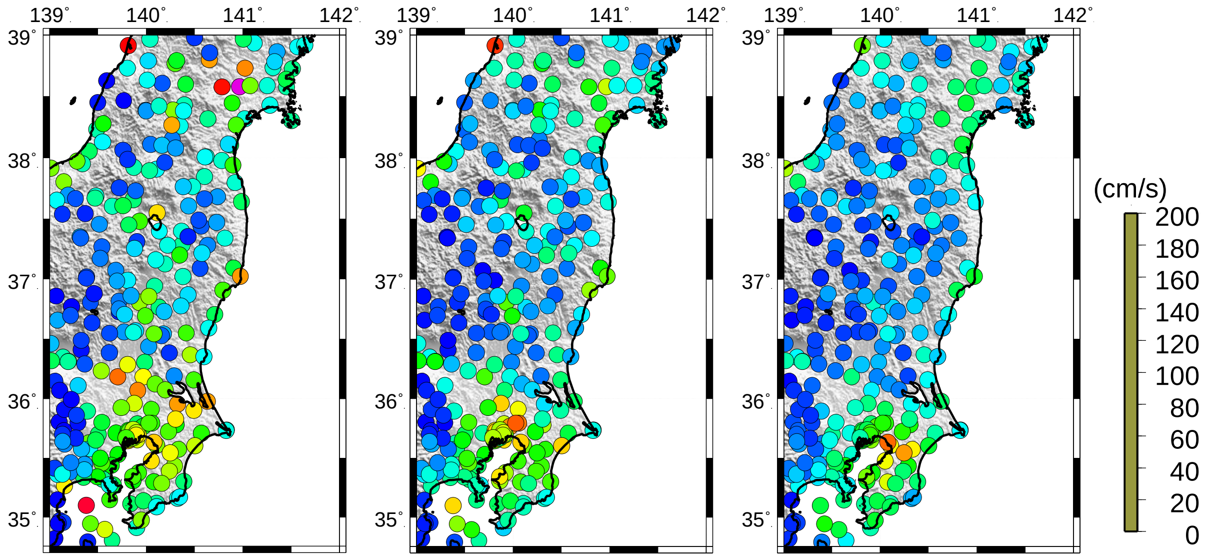

Figure 11. Pseudo-Velocity Response Spectra Observed at the K-NET and KiK-net Stations (EW comp., h=5%)

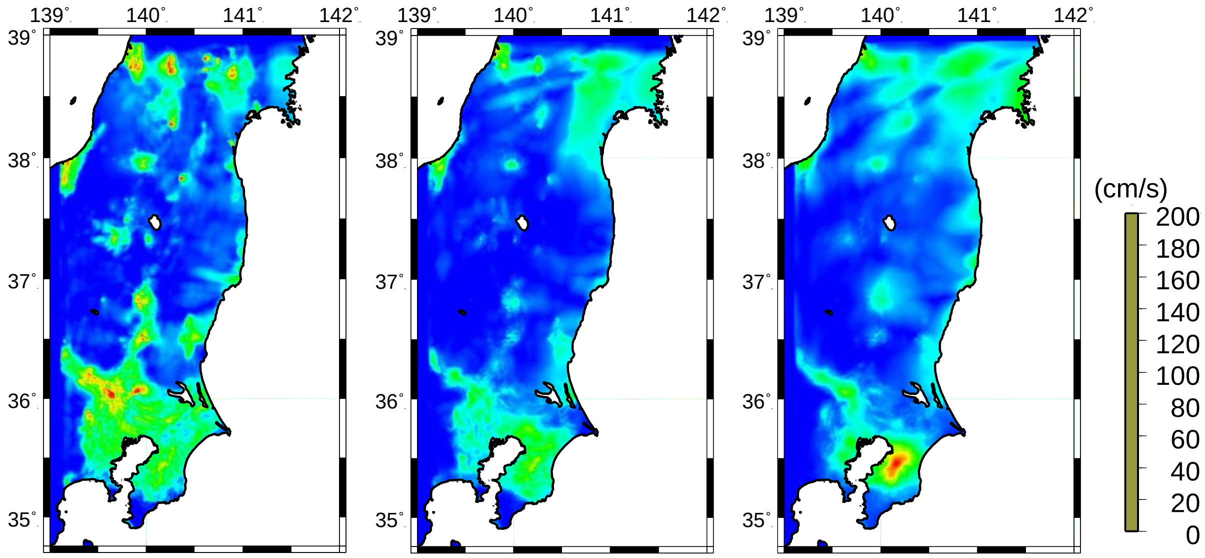

Figure 12. Pseudo-Velocity Response Spectra for Strong Ground Motion Simulation (EW comp., h=5%)

in the Kanto and Sendai basins, and this is fairly well reproduced in the calculated results shown in Fig. 12. However, careful examination of the spectra for a period of 10 sec shows that the calculations overestimate the observed ones in the west side of Tokyo Bay. This result suggests that the velocity and attenuation in the subsurface structure model needs to be reconsidered. In addition, Fig. 11 shows that for a period of 4 sec, large amplitudes were observed at many stations in regions other than the Kanto and Sendai basins, whereas this behavior was not replicated by the simulation. This is also most likely due to the fact that our simulation model did not account for the amplification of the surface structure.

5. CONCLUSIONS

In this study, the source model of the 2011 Tohoku earthquake was estimated, and seismic ground motions with periods of 3 to 10 sec were simulated using our source model and the subsurface structure model provided by HERP, and then the results were compared to the observed ground motions during the 2011 off the Pacific coast of Tohoku earthquake. The main findings were as follows:

For Source Modeling

(1) We proposed a source model composed of five SMGAs located in the sea off Miyagi, south Iwate, Fukushima and Ibaraki Prefectures. Using this source model,

(2) The observed waveforms are well reproduced by the synthetic waveforms calculated by the empirical Green's function method.

For Strong Ground Motion Simulation

(3) The propagation of seismic ground motion (such as the arrival time and duration) from the north into the Kanto basin were reproduced by the strong ground motion simulation.

(4) The amplitude of the principal motions and shapes of wave packet are reproduced from station MYGH12 in Miyagi Prefecture to IBR016 in Ibaraki Prefecture, but the later phase amplitudes of the synthetic waveforms were somewhat lower than that of the observed waveforms.

(5) At observation stations in the Kanto basin south of SIT010 in Saitama Prefecture, the amplitudes of the predicted waveforms are well reproduced by the synthetic waveforms. In addition, not only the amplitudes but also the phases of the UD components of the observed waveforms are well reproduced by the synthetic waveforms. However, the later phase amplitudes of the synthetic waveform are lower than the amplitudes observed at the stations in Kanto basin.

(6) In the horizontal component, large ground velocities were observed from stations in the Sendai basin and south Fukushima Prefecture along the coast into the Kanto basin. However, in the vertical component, the maximum velocities were relatively high in the Sendai Basin, whereas they were relatively low in the Kanto basin. The calculated results generally reproduced this trend.

(7) The observed pseudo-velocity response spectra showed large amplitudes in the Kanto and Sendai basins for periods of 7 and 10 sec, and the synthesized spectra generally reproduced this trend. However, the spectra for a period of 10 sec shows that the synthesized spectra overestimate in the west side of Tokyo Bay.

(8) The synthesized 4 sec response spectra underestimated in locations other than the Kanto and Sendai basins. Just as for the velocity spectra, this is possibly due to the fact that the subsurface structure model did not account for the wave amplification in the surface structure.

In this study, the subsurface structure model and our source model consisting of five SMGAs were employed to simulate ground motions. In future work, this simulation will be further refined by considering five SMGAs and the other regions of the source area, and reconsidering the subsurface structure model. It is hoped that this will provide a more accurate representation of the amplitude of the later phase, the phase of the principal motions, and other earthquake parameters.

ACKNOWLEDGEMENT

We thank the National Institute for Earth Science and Disaster Research (NIED), Japan for strong motion records, the Japan Meteorological Agency for the focal mechanism information, and the Headquarters for Earthquake Research Promotion of Japan for the subsurface structure model.

REFERENCES

Cerjan, C., Kosllof, D., Kosllof, R. and Reshef, M. (1985), A nonreflecting boundary condition for discrete acoustic and elastic boundary condition, *Geophysics*, **50**, 171-176.

Clayton, R. and Engquist, B. (1977), Absorbing boundary condition for acoustic and elastic wave equations. *Bull. Seism. Soc. Am.*, **67**, 1529-1540.

Graves, R. W. (1996), Simulating seismic wave propagation in 3D elastic media using staggered-grid finite differences. *Bull. Seism. Soc. Am.*, **86**, 1091-1106.

Irikura, K. (1986), Prediction of strong acceleration motion using empirical Green's function, *Proc. 7th Japan Earthquake Engineering Symposium, Tokyo*, 151-156.

Nakamura, H. and Miyatake, T. (2000), An approximate expression of slip velocity time function for simulation of near-field strong ground motion, *ZISIN*, **53:1**, 1-9. (in Japanese)

Pitarka, A. (1999), 3D finite-difference modeling of seismic motion using staggered grids with nonuniform spacing, *Bull. Seism. Soc. Am.*, **89**, 54-68.

The Headquarters for Earthquake Research Promotion of Japan (2012), Long-Period Ground Motion Hazard Map, http://www.jishin.go.jp/main/chousa/12_choshuki/ (in Japanese)

Wessel, P., and W. H. F. Smith (1995), New version of the Generic Mapping Tools released, *EOS*, **76**, 329.